PCCP

PAPER

View Article Online
View Journal | View Issue

Check for updates

Cite this: *Phys. Chem. Chem. Phys.*, 2025, **27**, 10875

On-surface chemistry of Pb(II) tetraphenylporphyrin on Au(111): reversible metalation, thermal degradation, and formation of a covalent organic framework†

Jan Herritsch, Cong Guo, Lukas J. Heuplick, Mark Hutter, Qitang Fan, Florian Münster, Stefan R. Kachel, Malte Zugermeier and J. Michael Gottfried *

Heavy-metal compounds play important roles in modern functional materials, enabling advancements in optoelectronics, catalysis, and beyond. Nanostructured surfaces incorporating heavy main group elements have shown significant promise for novel applications but often suffer from insufficient thermal stability. To address these challenges resulting from thermally induced reactions, we study the on-surface chemistry of Pb(II) 5,10,15,20-tetraphenylporphyrin, Pb(TPP), on the Au(111) surface as a model system. Pb(TPP) is formed either by vapor deposition of Pb atoms onto a monolayer of free-base tetraphenylporphyrin, H_2(TPP), or by direct deposition of pre-synthesized Pb(TPP). Using XPS and STM, we compare these Pb(TPP) monolayers and find that *in situ* metalation exclusively yields configurations in which the Pb atom points away from the surface (Pb↑). Thermal degradation of Pb(TPP) on Au(111) differs mechanistically from previously reported transmetalation on Cu(111). Below 550 K, the Pb atom in Pb(TPP) is replaced by hydrogen through demetalation, resulting in a reduction of the released Pb atom and formation of H_2(TPP). This process is enabled by cyclodehydrogenation of the TPP ligand, which releases the necessary hydrogen. Above 550 K, free-base porphyrins undergo remetalation with Au atoms from the substrate, while simultaneous C–H bond activation induces intermolecular coupling, resulting in the formation of two-dimensional covalent organic frameworks (COFs) of Au porphyrins. These porphyrin-based COFs with embedded metal centers exemplify a promising platform for surface-supported functional materials with MN_4 centers, paving the way for innovative applications in heterogeneous (electro)catalysis and related fields.

Received 31st January 2025,
Accepted 4th May 2025

DOI: 10.1039/d5cp00422e

rsc.li/pccp

Open Access Article. Published on 05 May 2025. Downloaded on 22/11/2025 12:13:35 AM.
This article is licensed under a Creative Commons Attribution 3.0 Unported Licence.

Introduction

Heavy main group elements (MGEs), which are characterized by unique properties such as relativistic effects and large spin–orbit splitting, tend to form stable metal–organic complexes.[1] Despite the lack of research on metal–organics of heavy MGEs, they represent promising building blocks for the assembly of novel optoelectronic materials, such as phosphorescent compounds with low optical bandgap and high charge mobility, which are advantageous for photovoltaic and thin-film transistor applications.[2] Moreover, nanostructured surfaces containing heavy MGEs have the potential to serve as effective single-site catalysts for the activation of small molecules.[3] Specifically, Pb metal–organics and covalent organic frameworks (COFs) based on Pb metal–organics as well as Pb single atom catalysts are applicable in the electrochemical CO_2 reduction reaction,[4,5] electrochemical two-electron oxygen reduction reaction,[6] the hydroamination of alkynes,[7] the cyanosilylation reaction[8] and the combustion of energetic compounds.[9] However, the decomposition of such a material could prove problematic. While it may reduce the catalytic activity, the release of Pb atoms could also have adverse environmental effects due to their toxicity. The related dynamic processes of MGE metal–organics at surfaces or interfaces (*e.g.*, chemical reactions, structural adaptation upon adsorption, decomposition, *etc.*) have remained largely unexplored so far.

Porphyrins are often used as building blocks for the assembly of nanostructured surfaces due to their ability to stabilize active metal centers within a rigid square-planar coordination environment.[10] Pb forms complexes with porphyrins, in which

Fachbereich Chemie, Philipps-Universität Marburg, Hans-Meerwein-Straße 4, 35043 Marburg, Germany. E-mail: gottfried@uni-marburg.de

† Electronic supplementary information (ESI) available: Background treatment of the Pb 4f XPS spectra; calculated valence electronic structure of Pb(TPP); further details on the adsorbate interactions of Pb(TPP) on Au(111); additional XPS spectra of the thermally induced on-surface reaction; details on the N 1s fitting procedure; STM images with comparison of the adsorbate structure of a Pb(TPP) monolayer after heating to 550 K and a H_2(TPP) monolayer on Au(111); additional XPS spectra of the on-surface metalation of H_2(TPP) with Pb and subsequent thermal degradation. See DOI: https://doi.org/10.1039/d5cp00422e

Open Access Article. Published on 05 May 2025. Downloaded on 22/11/2025 12:13:35 AM.
This article is licensed under a Creative Commons Attribution 3.0 Unported Licence.

the divalent central atom is situated within a square-pyramidal coordination environment outside the N_4 plane of the porphyrin ring.[11–13] This structure with an out-of-plane bound metal center is a consequence of the large radius of the Pb^{2+} ion, which typically results in a distance of approximately 1.2 Å between the N_4 plane and the Pb center.[14,15] As a result of the non-planar molecular structure and lower symmetry, the central atom is highly exposed, which gives rise to a distinctive coordination chemistry of Pb(II) porphyrins.[16–18] Due to this structure, Pb(II) porphyrin complexes are ideal for the incorporation of active Pb centers into a catalytically active surface structure. In related materials synthesis, it is common practice to subject the metalloporphyrin-based materials to a thermal treatment, for example pyrolysis, in order to obtain a durable and laterally cross-linked single-atom catalyst that maintains the metalloporphyrin's MN_4 functionality.[19,20] However, such an approach can promote undesirable decomposition such as an exchange reaction of the central atom.

Previously, the on-surface transmetalation of Pb(II) 5,10,15,20-tetraphenylporphyrin, Pb(TPP), on the Cu(111) surface *via* a Pb → Cu redox exchange under ultrahigh-vacuum (UHV) conditions was reported. It was demonstrated that the central Pb(II) atom is reduced and replaced by a Cu atom from the underlying Cu(111) substrate at moderate temperatures (380 K).[21]

While metal exchange and demetalation reactions have frequently been observed in solution or at solid–liquid interfaces,[22–24] where they proceed *via* a non-redox ion exchange mechanism, the situation is different in the absence of solvent, when ionic processes are disfavored. Therefore, metal exchange of metalloporphyrins on surfaces in UHV has rarely been observed.[25–28] Recently, it was postulated that Pd porphyrins can undergo a demetalation reaction on the Cu(100) surface in UHV, whereby the leaving Pd center is reduced. However, the formation of the free-base porphyrin with two inner NH protons was not observed, raising the question of the chemical state of the remaining porphyrin after demetalation.[29]

Here, we focus on the reversible metalation of 5,10,15,20-tetraphenylporphyrin, H_2(TPP), by vapor deposition of Pb atoms onto an adsorbed monolayer film on Au(111). Direct on-surface porphyrin metalation has previously been used for the preparation of transition-metal porphyrin complexes[30–33] and recent studies have shown that this method can also be applied to main group elements.[34] Specifically, we demonstrate that the on-surface metalation with Pb is reversible in the case of Pb(TPP) and that the free-base, H_2(TPP) is regained by thermal treatment. The replacement reaction of the Pb atom with two NH protons is monitored by X-ray photoelectron spectroscopy (XPS). Furthermore, the intact demetalation product, H_2(TPP), is unambiguously identified by mass spectrometry in a temperature-programmed desorption (TPD) experiment. The porphyrin demetalation requires H atoms, which are released by cyclodehydrogenation side-reactions of the TPP ligand backbone (Fig. 1). The different products of this side reaction are observed using scanning tunneling microscopy (STM). Heating to 700 K results in a two-dimensional (2D) covalent organic framework (COF) consisting of fused Au porphyrins, which are formed by remetalation of the linked porphyrins with Au adatoms. The reported reversible and irreversible coordination reactions provide valuable insights into the thermal evolution of metalloporphyrin-functionalized surfaces. Furthermore, the porphyrin-based 2D COF paves the way for the development of future functional materials, which are related to graphene-based materials with embedded N_4-metal centers, as frequently studied in (electro)catalysis and related applications.[35–37]

Experimental and computational details

All experiments were conducted under ultra-high vacuum (UHV) conditions, with a base pressure in the range of 10^{-10} mbar. The substrate used was an Au(111) single crystal (purity > 99.999%, MaTecK, Germany), which was cleaned by repeated cycles of Ar^+ ion bombardment (0.8 keV) followed by annealing (> 800 K). Surface cleanliness was confirmed by XPS prior to the XPS and STM experiments. XPS and STM were performed in a two-chamber UHV setup using a monochromatized Al Kα X-ray source (1486.7 eV) and a SPECS Phoibos 150 electron energy analyzer equipped with an MCD-9 multi channeltron detector as well as a SPECS Aarhus 150 STM. TPD experiments were carried out in a separate vacuum chamber using a HIDEN EPIC 1000 quadrupole mass spectrometer mounted inside a differentially pumped cryo shroud cooled to 90 K with l-N_2. The prepared sample was placed in front of the orifice

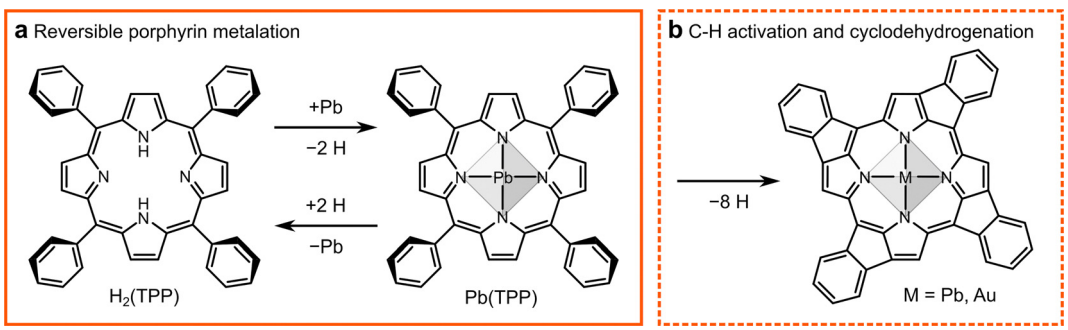

Fig. 1 (a) Reversible on-surface metalation of H_2(TPP). Reaction with Pb at 300 K yields Pb(TPP), which undergoes demetalation at elevated temperatures. (b) Thermal C–H activation and (cyclo)dehydrogenation. Only one possible product is shown. The released H atoms engage in the demetalation of Pb(TPP) as shown in (a).

 This journal is © the Owner Societies 2025

Open Access Article. Published on 05 May 2025. Downloaded on 22/11/2025 12:13:35 AM. This article is licensed under a Creative Commons Attribution 3.0 Unported Licence.

(8 mm diameter) of the cryo shroud and the crystal was heated resistively *via* tungsten wires with a constant rate of 1 K s^{-1}. Temperatures were measured using a calibrated type K thermocouple mounted inside the sample. H_2(TPP) (PorphyChem SAS, purity >98%), Pb(TPP) (Por-Lab, Porphyrin Laboratories GmbH, purity >95%), and Pb metal (Hauner Metallische Werkstoffe, purity >99.99%) were purchased from commercial sources. Substrate coverages θ are given as the number of adsorbed molecules divided by the number of substrate atoms. According to previous work,[38] a coverage of θ = 0.037 corresponds to a closed TPP monolayer. DFT calculations were performed with Gaussian16, A.03[39] using the PBE[40] functional. The def2-TZVPP[41–43] basis set was used for the light elements (N, C, H). For Pb, def2-TZVPP was used in combination with an effective core potential (def2-ECP)[44] to account for relativistic effects. The "tight" convergence criteria and an "ultrafine" integration grid were applied in this regard.

Results and discussion

Adsorbate structure of Pb(TPP) on Au(111)

Fig. 2(a) shows an STM image of a directly deposited Pb(TPP) monolayer. The molecules adopt a highly ordered and densely packed adsorbate structure. Some of the Pb(TPP) molecules appear with a bright center, while no protruding center can be observed in the rest of the molecules. These two distinct adsorption states can be attributed to the non-planar "shuttlecock" shape of Pb tetrapyrrole complexes, which can adsorb with the Pb atom pointing either toward the surface (Pb↓) or away from it (Pb↑). The formation of these two adsorbate geometries is characteristic of tetrapyrrole complexes with an out-of-plane bound metal center and has been previously reported *e.g.* for Sn(II) phthalocyanines, Sn(Pc),[45–48,80] and Pb(II) phthalocyanines, Pb(Pc).[49,79] Based on the STM image, the fraction of the Pb↑ isomer is estimated to be 29%.

Fig. 2(b) compares the Pb 4f spectrum of a directly deposited Pb(TPP) monolayer with that of a partially metalated H_2(TPP) monolayer, a Pb(TPP) multilayer (4.0 nm film thickness, corresponding to 13 layers), and a metallic Pb(0) reference on Au(111). In case of the monolayer spectra, the signal from the pristine Au(111) substrate was subtracted as a background correction (see Fig. S1 in the ESI† for details). The Pb 4f signal of a directly deposited Pb(TPP) monolayer exhibits a broad asymmetric shape for both spin–orbit components. The Pb $4f_{7/2}$ signal is described using a fit with two peaks at 137.5 eV and 138.3 eV, corresponding to the coexistence of two distinct Pb(II) states, which reflect the two different adsorption geometries of Pb(TPP) (Pb↑ and Pb↓). The Pb↓ geometry is assigned to the Pb $4f_{7/2}$ peak at 137.5 eV, with the reduced binding energy (BE) attributed to an increased core–hole screening. In contrast, the Pb $4f_{7/2}$ peak at 138.3 eV corresponds to the Pb↑ geometry and is slightly shifted to higher binding energies compared to the Pb(II) state in the multilayer (137.9 eV). This shift can be explained by an intramolecular charge rearrangement, as previously discussed for the Sn↑ isomer of Sn(II) phthalocyanines on Ag(111).[45] According to the Pb $4f_{7/2}$ signal intensities, about 68% of the Pb(TPP) molecules adsorb in the Pb↓ geometry, while 32% adopt the Pb↑ configuration. The Pb↑ fraction derived from the Pb $4f_{7/2}$ signal is in good agreement with the STM images (29% Pb↑). The unequal distribution of Pb↑ and Pb↓ molecules may be due to details of the adsorption process, especially different sticking probabilities of Pb(TPP) in the Pb↑ and Pb↓ states. Related imbalances have previously been observed *e.g.* for the shuttlecock-shaped Pb(Pc), which forms almost pure Pb↑ islands on Pb films on Ag(111), while equal amounts of Pb↑ and Pb↓ were found on Ag(111).[49] Interestingly, the Pb 4f spectrum of the partially metalated H_2(TPP) monolayer suggests that on-surface metalation exclusively yields the Pb↑ isomer, as will be discussed in more detail below.

The appearance of Pb(TPP) in STM images exhibits a distinct dependence on the tunneling voltage, as can be seen in Fig. 2(c)–(e). The bright protrusion of the Pb↑ isomer is only

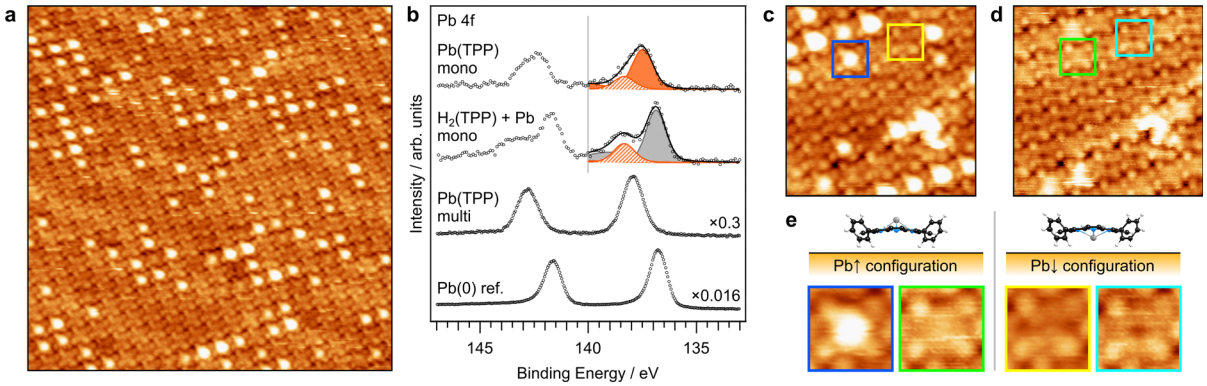

Fig. 2 (a) STM image of a Pb(TPP) monolayer showing an ordered adsorbate structure in which two adsorption configurations (Pb↑ and Pb↓) coexists. (b) Pb 4f spectra of a directly deposited Pb(TPP) monolayer, a partially metalated H_2(TPP) monolayer by deposition of Pb atoms, a Pb(TPP) multilayer, and a Pb(0) reference on Au(111). The Pb $4f_{7/2}$ region of the monolayer spectra is described by a fit function of Pb(TPP) colored in orange with the Pb↑ isomer shown hatched as well as the signal of unreacted Pb(0) atoms colored in gray. (c,d) STM images of the same surface are, scanned with negative (left) and positive (right) bias voltage. Pb↑ and Pb↓ configurations show different appearances depending on the tunneling bias. (e) Image sections from (c), (d) showing the Pb↑ and Pb↓ isomers. Tunneling parameters and image size: (a) U = −1.20 V, I = −0.16 nA, 30 × 30 nm^2; (c) U = −1.20 V, I = −0.09 nA, 10 × 10 nm^2; (d) U = +1.20 V, I = +0.09 nA, 10 × 10 nm^2, (e) U = +1.20 V, I = +0.09 nA, 1.8 × 1.8 nm^2.

Open Access Article. Published on 05 May 2025. Downloaded on 22/11/2025 12:13:35 AM.
This article is licensed under a Creative Commons Attribution 3.0 Unported Licence.

seen by screening the occupied states (negative tunneling bias); otherwise, the molecule's center appears flat. A detailed examination of the STM images reveals that the Pb↑ molecules display centers of varying apparent height, which may be attributed to minor alterations in the adsorption sites of the individual molecules. This phenomenon could be related to the herringbone reconstruction of the Au(111) surface. The bright contrast of the metal center in the Pb↑ isomer can be attributed to the valence electronic structure, which is discussed in detail in Section S2 in the ESI† using gas-phase DFT calculations. Based on a calculated Au·Pb(TPP) complex and literature findings for Sn(Pc) on Ag(111)[50,51] a covalent interaction between the Pb↓ center and the Au substrate is proposed as discussed in Section S3 of the ESI.† Although no experimental evidence for a partial oxidation of the Pb(II) center upon adsorption is available, DFT suggests a covalent donor bond between the Pb(TPP) HOMO–2 and the Au 6s orbital of the substrate.

On-surface demetalation of Pb(TPP)

The temperature-induced demetalation of Pb(TPP) was studied using a directly deposited monolayer on Au(111). The Pb(TPP) monolayer sample was successively heated to different temperatures, which were kept for five minutes, and afterwards investigated using XPS and STM. Fig. 3(a) shows XPS spectra for selected temperatures. Data for intermediate heating steps are depicted in Fig. S4 in the ESI.† The N 1s spectra in Fig. 3(a) and Fig. S4 in the ESI† reveal the thermal transformation of the porphyrin's N_4 coordination site. The initial Pb(TPP) monolayer exhibits a single N 1s peak at 397.8 eV representing the intact complex with four chemically equivalent N atoms, in line with the typical N 1s signature of porphyrin complexes.[52] After heating the sample, a second feature evolves at higher binding energies, which is attributed to a pyrrolic N atom (N–H). The presence of a pyrrolic N–H species indicates that a demetalation has occurred and that the central Pb atom is replaced by two H atoms yielding H_2(TPP). The degree of exchange of Pb with two H atoms can be estimated by a fit function using a pyrrolic (N–H) and an iminic (–N=) component in a 1 : 1 ratio. Details on the used fit model can be found in Section S5 in the ESI.† Upon heating to 550 K, a complete demetalation was achieved. Above 570 K, a further transformation of the N 1s signal into a single peak at 398.1 eV indicates that again a metalloporphyrin complex was formed, as confirmed by the four chemically equivalent N atoms.

As the demetalation of Pb(TPP) is a redox reaction in which the leaving Pb(II) center is reduced, the reaction can be also monitored based on the change of the Pb oxidation state, which is assessed by the Pb $4f_{7/2}$ spectra shown in Fig. 3(a) and additional data in Fig. S4 in the ESI.† At temperatures at and above 470 K, the Pb $4f_{7/2}$ peak becomes narrower and shifts to lower binding energies, which can be described using a fit model based on the signature of a Pb(0) reference. Heating the sample to temperatures above 570 K does not change in the Pb oxidation state, indicating that reaction at high temperatures does not result in a reformation of a Pb(II) complex. Therefore, it is proposed that a Au porphyrin complex is formed by reaction with Au adatoms. Such metalation of free-base porphyrins with predeposited metal atoms or substrate metal atoms (self-metalation) has previously been observed for Zn,[53] Cu,[52,54–64] Ag,[65] and Au.[66–68]

Fig. 3(b) and (c) show the temperature-dependent normalized N 1s and the Pb $4f_{7/2}$ intensities, providing information

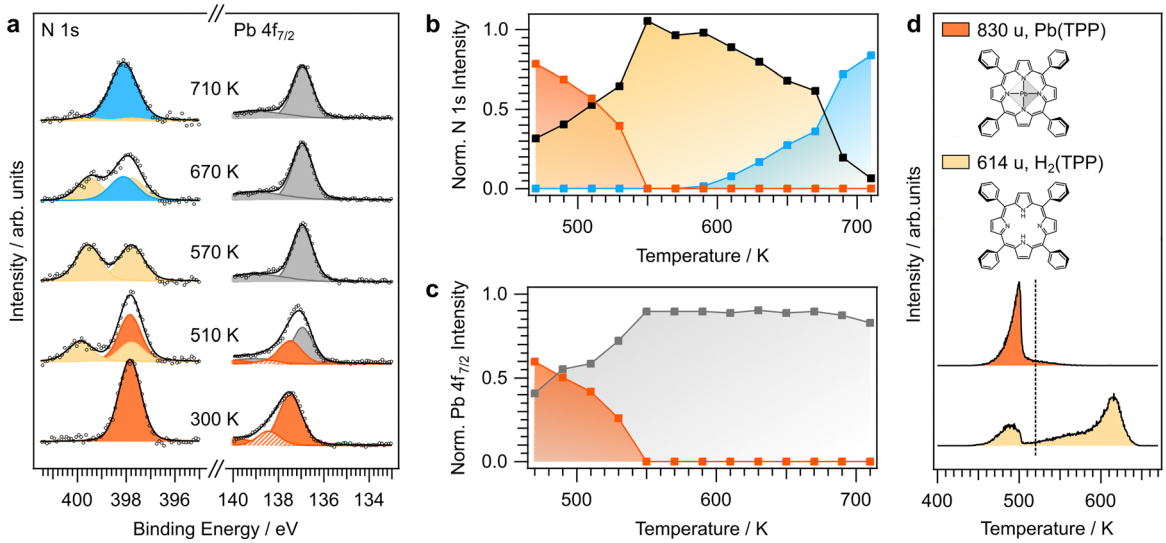

Fig. 3 (a) N 1s and (b) Pb $4f_{7/2}$ XPS spectra of a Pb(TPP) monolayer before (bottom spectra) and after annealing to the indicated temperatures. The intermediate heating steps of the complete series are given in Fig. S4 in the ESI.† The fit of the N 1s region includes the components Pb(TPP) (orange), the demetalation product H_2TPP (yellow), and Au porphyrin complexes (blue). The fit of the Pb 4f region includes the components Pb(II) from Pb(TPP) (orange; the Pb↑ isomer hatched) and Pb(0) (gray). (b) Temperature-dependent intensities of the components Pb(TPP), free-base porphyrins, and Au porphyrins, as obtained from the N 1s spectra in (a). (c) Temperature-dependent intensities of the components Pb(II) and Pb(0), as obtained from the Pb $4f_{7/2}$ spectra in (a). (d) TPD traces for 614 u (H_2(TPP)) and 830 u (Pb(TPP)) for a thin Pb(TPP) multilayer. Desorption of the multilayer occurs below 520 K (dashed line), while the signal at higher temperatures is attributed to the partial desorption of the monolayer.

 This journal is © the Owner Societies 2025

Open Access Article. Published on 05 May 2025. Downloaded on 22/11/2025 12:13:35 AM.
This article is licensed under a Creative Commons Attribution 3.0 Unported Licence.

about the transformation of the porphyrin's N_4 coordination site and the reduction of the Pb(II) central atom. The reduction of Pb(II) and demetalation of the porphyrin rings show the same temperature dependency, which is line with the postulated reaction: Pb(TPP) + 2H → H_2(TPP) + Pb. However, the reaction requires H atoms which stem from the dehydrogenation side-reaction of the TPP ligand. The details of this side-reaction are further examined below using STM.

To confirm the formation of free-base H_2TPP, a TPD mass spectrometry experiment was performed. Fig. 3(d) shows the TPD traces for the masses 614 u (H_2(TPP)) and 830 u (Pb(TPP)) for a thin multilayer. Below 520 K, desorption of intact Pb(TPP) from the multilayer is dominant. Above 520 K, only desorption of H_2(TPP) is observed during partial desorption of the monolayer, indicating that the product of the thermally induced degradation of Pb(TPP) on Au(111) is indeed the free-base tetraphenylporphyrin, in line with the XPS results. The reaction requires H atoms, which replace the Pb central atom. Note that small amounts of H_2(TPP) are observed already below 520 K, which could partly be caused by a superposition of the H_2(TPP) signal ($C_{44}H_{30}N_4$, 614 u) with the signal of the TPP fragment formed in the ion source of the mass spectrometer due to the loss of the central Pb atom. (The calculated isotopic pattern of TPP ($C_{44}H_{28}N_4$) is as follows: *m*/*z* (calc.) 612.23 (100.0%), 613.23 (49.1%), 614.24 (11.2%), 615.24 (1.9%)). However, this cannot be the only source of the H_2(TPP) intensity, because the signal shapes deviate, indicating that there is actual desorption of H_2(TPP). Therefore, it is concluded that H_2(TPP) is already formed below 520 K, in line with the XPS results. Desorption of the H_2(TPP), which was formed in the monolayer, together with the multilayer, is enabled by exchange of molecules between monolayer and multilayer during desorption, as was previously reported for phthalocyanines.[69]

To clarify the origin of the H atoms for the demetalation, it is necessary to assess the relationship between the porphyrin demetalation and the dehydrogenation side-reaction of the TPP ligand. For this aim, the non-desorbing reaction products are examined in more detail using STM.

Fig. 4(a) shows an STM image of a Pb(TPP) monolayer after annealing to 550 K. According to XPS, the demetalation is complete at this temperature and the porphyrin rings are present solely in the free-base form, *i.e.*, all macrocycles contain two inner N–H hydrogen atoms. In contrast to the STM images of the initial Pb(TPP) monolayer at 300 K (Fig. 2(a)), no molecules with protruding center are visible, indicating that the presence of Pb(TPP) in the Pb↑ isomer can be excluded, in agreement with the XPS results. The STM images also show a slight decrease in coverage. In the vicinity of the vacancy areas, some molecules are found that exhibit an altered structure of the TPP ligand backbone (Fig. 4, colored boxes). A thorough examination of their structures enables the assignment of selected molecules to different species. Fig. 4(b) shows the intact demetalation product, H_2(TPP), as evident from a comparison with H_2(TPP) that was directly deposited on Au(111), shown in Fig. S6 in the ESI.† The structures in Fig. 4(c)–(e) are assigned to different cyclodehydrogenation products of the TPP ligand, which were discussed previously.[70,71] This side-reaction leads to the formation of various products, as each of the four phenyl substituents can undergo one of two possible intramolecular coupling reactions with the neighboring *meso*-carbons of the porphyrin macrocycle. The selected structures in Fig. 4(b)–(e) represent only one possible reaction pattern, and alternative coupling patterns can also be observed. The STM images thus confirm that the ligand's side-reaction takes place simultaneously with the demetalation. The H atoms released by the TPP dehydrogenation are therefore available for the formation of H_2(TPP).

A competing process to the observed porphyrin demetalation and formation of H_2(TPP) is the desorption of the released hydrogen. Previous TPD studies have shown that the recombinative desorption of hydrogen as H_2 occurs around 110 K on the Au(111) surface.[72] Desorption of H atoms does not play a

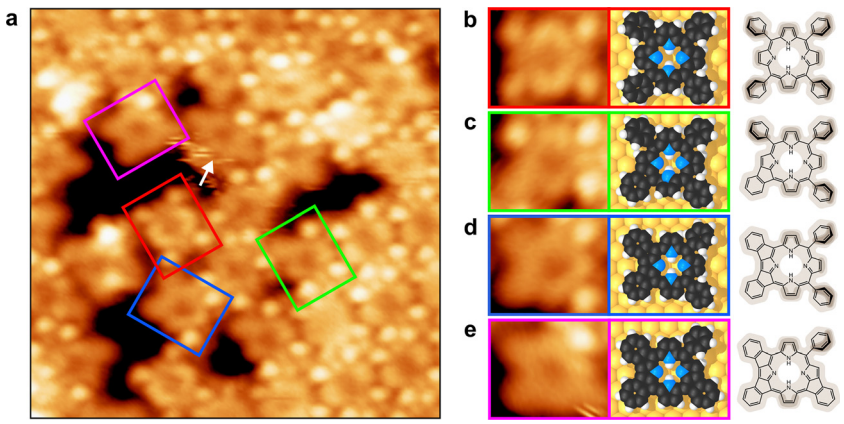

Fig. 4 (a) STM image of a Pb(TPP) monolayer on Au(111) after annealing to 550 K, revealing the formation of the intact demetalation product H_2(TPP) (red box) as well as various cyclodehydrogenation products (green, blue and purple boxes). (b)–(e) Enlarged image sections of selected molecules, proposed adsorbate structure, and corresponding molecular structures with shadings highlighting protruding parts. The selected structures in (b)–(e) illustrate one of several possible reaction pathways of the ligand's side reaction. Products with alternative coupling patterns can also be observed (*e.g.* in (a), see white arrow). Tunneling parameters and image size: (a) $U = -1.40$ V, $I = -0.14$ nA, 10 × 10 nm^2.

Open Access Article. Published on 05 May 2025. Downloaded on 22/11/2025 12:13:35 AM. This article is licensed under a Creative Commons Attribution 3.0 Unported Licence.

significant role because of the high adsorption energy of atomic H on Au(111) of around −2 eV, as calculated by DFT.[73] The diffusion barrier for H atoms on Au(111) is 0.30 eV, which is in line with the observed temperature of recombinative desorption.[74] Nonetheless, it has been shown that H atoms on Au(111) engage in various reactions besides recombinative desorption and can effectively be used in on-surface synthesis. This includes H atoms formed by dehydrogenation reactions as well as H atoms dosed with the hydrogen cracker. For example, it has frequently been observed that H atoms released by dehydrogenation processes react with residual Br atoms from the Ullmann coupling, resulting in the desorption of HBr. Desorption of H_2 occurs only after all Br has been consumed.[75] Hydrogen atoms produced by a hydrogen cracker were used for removal of halogen residues from the surface after Ullmann coupling, to convert organometallic compounds to hydrogenated species, and as a reagent for debromination or desulfurization of adsorbed molecules.[76] Furthermore, it has been shown that H atoms can catalyze the dehydrogenation of nanographene precursors.[77] In light of these previous examples, it is not surprising that H atoms can also participate in the demetalation of Pb(TPP), resulting in the formation of H_2(TPP).

Porphyrin remetalation with Au atoms and formation of a 2D covalent organic framework

The N 1s XPS spectra in Fig. 3(a) have already shown that remetalation of the previously demetalated porphyrin ring takes place above 600 K. Fig. 5(a) shows an STM image of the Pb(TPP) monolayer after heating to 700 K. The coverage has slightly deceased and the entire surface is characterized by a higher degree of heterogeneity. Instead of individual molecules, covalently cross-linked moieties forming a disordered 2D framework are observed. Therefore, the thermal degradation of Pb(TPP) at 700 K not only leads to intramolecular cyclodehydrogenation reactions, but also to intermolecular coupling. Moreover, the porphyrin units in the network contain a brightly protruding center, indicating a remetalation in agreement with the XPS results in Fig. 3(a). In accordance with previous literature on the on-surface metalation of free-base porphyrins,[52–68] it is concluded that the initially formed free-base porphyrin derivatives react with Au atoms from the underlying Au(111) substrate yielding Au porphyrin complexes. The close-up STM image in Fig. 5(b) shows round protrusions between the fused Au porphyrin rings, which are attributed to Pb(0) atoms that were released during the preceding demetalation of Pb(TPP). The fact that the Pb atoms remain on the surface is consistent with the insolubility of Pb in Au below 800 K.[78]

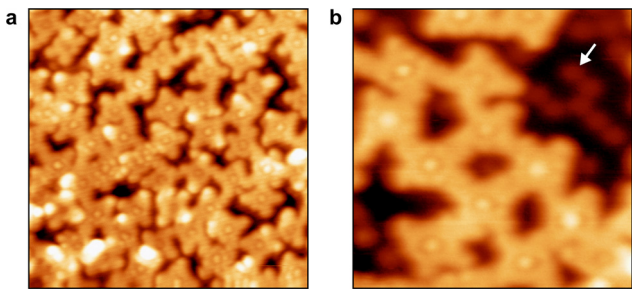

Fig. 5 STM images taken after heating a Pb(TPP) monolayer on Au(111) to 700 K, showing formation of a 2D covalent organic framework of Au porphyrins. (a) Overview image. The framework extends over the entire surface. (b) Zoom-in STM image, showing the protruding center of the porphyrin rings caused by the ligated Au atoms. Areas between the fused Au porphyrins contain round protrusions (marked by the white arrow), which are attributed to Pb(0) atoms released during the demetalation of Pb(TPP). Tunneling parameters and image sizes: (a) U = −0.56 V, I = −0.15 nA, 10 × 10 nm^2; (b) U = −2.22 V, I = −0.24 nA, 5 × 5 nm^2.

The thermally induced reactivity of Pb(TPP) on Au(111) is found to differ significantly from the previously reported on-surface *trans*-metalation of Pb(TPP) on Cu(111).[21] On Au(111), the leaving of the Pb atom and the entering of the substrate's Au atom occur in two different temperature ranges, which have no overlap (see Fig. 3(c)). This phenomenon can be attributed to the presence of H atoms, which are released by the cyclodehydrogenation side-reaction of the TPP ligand, thereby enabling the demetalation. In addition, our results also differ from the recently postulated demetalation of Pd porphyrins on the Cu(100) surface,[29] where no evidence for a demetalated free-base porphyrin species was found.

On-surface metalation of H_2(TPP) with Pb

To achieve the on-surface synthesis of the Pb(TPP) complex, Pb atoms were deposited on a H_2(TPP) monolayer, which was obtained by partial desorption of a thin multilayer (thickness ∼6 layers) *via* heating the sample to 520 K for 3 min. During the deposition of Pb, the sample was kept at 300 K. The amount of Pb atoms corresponds to a coverage of θ = 0.086, which is approximately two Pb atoms per H_2(TPP) molecule in the initial monolayer and, thus, represents a two-fold excess with respect to the formation of Pb(TPP).

The XPS spectrum of the metalation product shows two separate Pb $4f_{7/2}$ peaks at 136.9 eV and 138.3 eV (Fig. 2(a)). The signal at lower BE is assigned to unreacted Pb(0) atoms, based on a Pb(0) reference spectrum, while the peak at higher BE corresponds to the actual metalation product, Pb(TPP). Accordingly, only a partial metalation of H_2(TPP) could be achieved, despite the excess of Pb, which agrees with the corresponding N 1s spectra showing that only approximately 50% of the free-base porphyrin is converted (see also Fig. S6 in the ESI†).

The comparison of the Pb $4f_{7/2}$ signals of the Pb(TPP) formed by *in situ* metalation of H_2(TPP) and the directly deposited Pb(TPP) monolayer shows that the on-surface metalation of H_2(TPP) yields the Pb↑ product exclusively. The underlying mechanism cannot be inferred directly from the data. However, it is likely that the large Pb atoms cannot penetrate the N_4 cavity of the porphyrin and that the entire molecule cannot flip over, *i.e.*, that no conversion between Pb↑ and Pb↓ isomer is possible under the experimental conditions. Therefore, the preferred formation of the Pb↑ species is attributed to the fact that the porphyrin ligand is not accessible to Pb atoms from the side of the surface. Due to the large atomic radius of Pb, it seems plausible that the formation of the Pb↓ product by the on-surface metalation is inhibited, since a

 This journal is © the Owner Societies 2025

Open Access Article. Published on 05 May 2025. Downloaded on 22/11/2025 12:13:35 AM. This article is licensed under a Creative Commons Attribution 3.0 Unported Licence.

diffusion of Pb atoms between porphyrin and substrate would require the complete porphyrin ring to be lifted from the Au surface. Therefore, the Pb atoms have to migrate on top of the TPP monolayer in order to reach the porphyrin's N_4 center. The relatively low yield of the reaction (compared to metalation with transition metal, which often show almost complete conversion[10,30,52]) and the high amount of unreacted Pb(0) could be due to the limited mobility of the Pb atoms on top of the organic monolayer film. Another important aspect in the exclusive formation of the Pb↑ configuration is that Pb atoms in direct contact with the Au substrate may not be reactive enough for the metalation of H_2(TPP).

Heating the *in situ* metalated H_2(TPP) film above 400 K initiates an on-surface degradation process, as can be seen by the temperature-dependent XPS spectra shown in Fig. S7 in the ESI.† This thermally induced degradation of Pb(TPP) results in a reduction of the central Pb atom and a change in the ligand's N_4 binding site. This on-surface reaction is discussed in detail below for the directly deposited Pb(TPP) monolayer.

Conclusion

In conclusion, we have examined the formation of Pb(TPP) by direct metalation of H_2(TPP) on the Au(111) surface, and the complex thermally induced degradation of Pb(TPP). The on-surface metalation of H_2(TPP) by vapor-deposition of Pb onto a monolayer of the porphyrin produces exclusively the Pb↑ isomer. Above room temperature, the Pb(TPP) monolayer on Au(111) undergoes complex degradation reactions. Below 550 K, demetalation and formation of the free-base H_2(TPP) is observed, as was confirmed by XPS and mass spectrometry. The replacement of the central Pb atom by two H atoms requires free H atoms, which are formed by parallel cyclodehydrogenation side-reactions of the TPP ligand. The cyclodehydrogenation results in intra- and intermolecular C–C coupling, which eventually yields a porphyrin-derived 2D covalent organic framework (COF). The porphyrin units in this framework undergo remetalation with Au adatoms from the substrate above 550 K. The resulting porphyrin-based COF is an intriguing model case for the porphyrin-derived carbon materials with MN_4 centers and paves the way for the development of future surface-supported metal–organic functional materials.

Author contributions

J. Herritsch: conceptualization, methodology, investigation, validation, formal analysis, writing – original draft, writing – review & editing. Cong Guo: investigation, visualization, formal analysis. Lukas J. Heuplick: investigation. Mark Hutter: investigation. Qitang Fan: investigation, visualization, formal analysis. Florian Münster: investigation. Stefan R. Kachel: investigation, visualization. Malte Zugermeier: investigation. J. Michael Gottfried: conceptualization, methodology, supervision, project administration, funding acquisition, resources, writing – review & editing.

Data availability

The data supporting this article have been included as part of the ESI.†

Conflicts of interest

There are no conflicts to declare.

Acknowledgements

Financial support by the Deutsche Forschungsgemeinschaft (DFG, German Research Foundation) through the CRC 1083 "Structure and Dynamics of Internal Interfaces" (223848855-SFB1083), the DFG grant GO1812/4-1, and by the State of Hessen through the LOEWE Focus Group PriOSS is gratefully acknowledged.

References

1 S. Arunkumar, D. Ghosh and G. R. Kumar, *Results Chem.*, 2022, **4**, 100399.
2 S. M. Parke, M. P. Boone and E. Rivard, *Chem. Commun.*, 2016, **52**, 9485–9505.
3 K. Oberdorf and C. Lichtenberg, *Chem. Commun.*, 2023, **59**, 8043–8058.
4 T. Zheng, C. Liu, C. Guo, M. Zhang, X. Li, Q. Jiang, W. Xue, H. Li, A. Li, C.-W. Pao, J. Xiao, C. Xia and J. Zeng, *Nat. Nanotechnol.*, 2021, **16**, 1386–1393.
5 Y. Xu, X. Liu, M. Jiang, B. Chi, Y. Lu, J. Guo, Z. Wang and S. Cui, *J. Colloid Interface Sci.*, 2024, **665**, 365–375.
6 X. Zhou, Y. Min, C. Zhao, C. Chen, M. K. Ke, S. L. Xu, J. J. Chen, Y. Wu and H. Q. Yu, *Nat. Commun.*, 2024, **15**, 193.
7 A. Chandran, J. M. Léon Baeza, V. Timofeeva, R. Nougué, S. Takahashi, R. Ohno, A. Baceiredo, R. S. Rojas Guerrero, M. Syroeshkin, T. Matsuo, N. Saffon-Merceron and T. Kato, *Inorg. Chem.*, 2022, **61**, 16156–16162.
8 A. Karmakar, S. Hazra, M. F. Guedes da Silva and A. J. Pombeiro, *Dalton Trans.*, 2015, **44**, 268–280.
9 W. Qu, S. Niu, D. Sun, H. Gao, Y. Wu, Z. Yuan, X. Chen, Y. Wang, T. An, G. Wang and F. Zhao, *Adv. Sci.*, 2021, **8**, 2002889.
10 J. M. Gottfried, *Surf. Sci. Rep.*, 2015, **70**, 259–379.
11 P. Sayer, M. Gouterman and C. R. Connell, *Acc. Chem. Res.*, 1982, **15**, 73–79.
12 O. Q. Munro, J. C. Bradley, R. D. Hancock, H. M. Marques, F. Marsicano and P. W. Wade, *J. Am. Chem. Soc.*, 2002, **114**, 7218–7230.
13 T. Yamaki and K. Nobusada, *J. Phys. Chem. A*, 2003, **107**, 2351–2355.
14 K. M. Barkigia, J. Fajer, A. D. Adler and G. J. B. Williams, *Inorg. Chem.*, 1980, **19**, 2057–2061.
15 M. J. Plater, S. Aiken, T. Gelbrich, M. B. Hursthouse and G. Bourhill, *Polyhedron*, 2001, **20**, 3219–3224.
16 C. M. Lemon, P. J. Brothers and B. Boitrel, *Dalton Trans.*, 2011, **40**, 6591–6609.

Open Access Article. Published on 05 May 2025. Downloaded on 22/11/2025 12:13:35 AM. This article is licensed under a Creative Commons Attribution 3.0 Unported Licence.

17 S. Le Gac and B. Boitrel, *J. Porphyrins Phthalocyanines*, 2016, **20**, 117–133.
18 F. Dai, W. Fan, J. Bi, P. Jiang, D. Liu, X. Zhang, H. Lin, C. Gong, R. Wang, L. Zhang and D. Sun, *Dalton Trans.*, 2016, **45**, 61–65.
19 S. Brüller, H.-W. Liang, U. I. Kramm, J. W. Krumpfer, X. Feng and K. Müllen, *J. Mater. Chem. A*, 2015, **3**, 23799–23808.
20 Y. Cao, Y. Mou, J. Zhang, R. Zhang and Z. Liang, *Mater. Today Catal.*, 2024, **4**, 100044.
21 J. Herritsch, S. R. Kachel, Q. Fan, M. Hutter, L. J. Heuplick, F. Münster and J. M. Gottfried, *Nanoscale*, 2021, **13**, 13241–13248.
22 M. Franke, F. Marchini, N. Jux, H.-P. Steinrück, O. Lytken and F. J. Williams, *Chem. – Eur. J.*, 2016, **22**, 8520–8524.
23 C. C. Fernández, M. Franke, H.-P. Steinrück, O. Lytken and F. J. Williams, *Langmuir*, 2021, **37**, 852–857.
24 C. C. Fernández, D. Wechsler, O. Lytken, H.-P. Steinrück and F. J. Williams, *Surf. Sci.*, 2022, **717**, 122005.
25 C. M. Doyle, J. P. Cunniffe, S. A. Krasnikov, A. B. Preobrajenski, Z. Li, N. N. Sergeeva, M. O. Senge and A. A. Cafolla, *Chem. Commun.*, 2014, **50**, 3447–3449.
26 D. Hötger, P. Abufager, C. Morchutt, P. Alexa, D. Grumelli, J. Dreiser, S. Stepanow, P. Gambardella, H. F. Busnengo, M. Etzkorn, R. Gutzler and K. Kern, *Nanoscale*, 2018, **10**, 21116–21122.
27 K. Shen, B. Narsu, G. Ji, H. Sun, J. Hu, Z. Liang, X. Gao, H. Li, Z. Li, B. Song, Z. Jiang, H. Huang, J. W. Wells and F. Song, *RSC Adv.*, 2017, **7**, 13827–13835.
28 G. Fratesi, D. Paoloni, L. Persichetti, L. Camilli, A. Caporale, A. Baby, D. Cvetko, G. Kladnik, A. Morgante and A. Ruocco, *Inorg. Chim. Acta*, 2024, **559**, 121790.
29 S. Baronio, M. Bassotti, F. Armillotta, E. Frampton, N. A. Vinogradov, L. Schio, L. Floreano, A. Verdini and E. Vesselli, *Nanoscale*, 2024, **16**, 13416–13424.
30 K. Diller, A. C. Papageorgiou, F. Klappenberger, F. Allegretti, J. V. Barth and W. Auwärter, *Chem. Soc. Rev.*, 2016, **45**, 1629–1656.
31 J. M. Gottfried, K. Flechtner, A. Kretschmann, T. Lukasczyk and H.-P. Steinrück, *J. Am. Chem. Soc.*, 2006, **128**, 5644–5645.
32 T. E. Shubina, H. Marbach, K. Flechtner, A. Kretschmann, N. Jux, F. Buchner, H.-P. Steinrück, T. Clark and J. M. Gottfried, *J. Am. Chem. Soc.*, 2007, **129**, 9476–9483.
33 P. Borghetti, G. Di Santo, C. Castellarin-Cudia, M. Fanetti, L. Sangaletti, E. Magnano, F. Bondino and A. Goldoni, *J. Chem. Phys.*, 2013, **138**, 144702.
34 A. Baklanov, M. Garnica, A. Robert, M. L. Bocquet, K. Seufert, J. T. Küchle, P. T. P. Ryan, F. Haag, R. Kakavandi, F. Allegretti and W. Auwärter, *J. Am. Chem. Soc.*, 2020, **142**, 1871–1881.
35 H. Yang, R. Shi, L. Shang and T. Zhang, *Small Struct.*, 2021, **2**, 2100007.
36 A. Facchin and C. Durante, *Adv. Sustainable Syst.*, 2022, **6**, 2200111.
37 S. Gu, A. N. Marianov, T. Lu and J. Zhong, *Chem. Eng. J.*, 2023, **470**, 144249.
38 T. Lukasczyk, K. Flechtner, L. R. Merte, N. Jux, F. Maier, J. M. Gottfried and H.-P. Steinrück, *J. Phys. Chem. C*, 2007, **111**, 3090–3098.
39 M. J. Frisch, G. W. Trucks, H. B. Schlegel, G. E. Scuseria, M. A. Robb, J. R. Cheeseman, G. Scalmani, V. Barone, G. A. Petersson, H. Nakatsuji, X. Li, M. Caricato, A. V. Marenich, J. Bloino, B. G. Janesko, R. Gomperts, B. Mennucci, H. P. Hratchian, J. V. Ortiz, A. F. Izmaylov, J. L. Sonnenberg, D. Williams-Young, F. Ding, F. Lipparini, F. Egidi, J. Goings, B. Peng, A. Petrone, T. Henderson, D. Ranasinghe, V. G. Zakrzewski, J. Gao, N. Rega, G. Zheng, W. Liang, M. Hada, M. Ehara, K. Toyota, R. Fukuda, J. Hasegawa, M. Ishida, T. Nakajima, Y. Honda, O. Kitao, H. Nakai, T. Vreven, K. Throssell, J. J. A. Montgomery, J. E. Peralta, F. Ogliaro, M. J. Bearpark, J. J. Heyd, E. N. Brothers, K. N. Kudin, V. N. Staroverov, T. A. Keith, R. Kobayashi, J. Normand, K. Raghavachari, A. P. Rendell, J. C. Burant, S. S. Iyengar, J. Tomasi, M. Cossi, J. M. Millam, M. Klene, C. Adamo, R. Cammi, J. W. Ochterski, R. L. Martin, K. Morokuma, O. Farkas, J. B. Foresman and D. J. Fox, *Gaussian 16, Revision A.03*, Gaussian, Inc., Wallingford CT, 2016.
40 J. P. Perdew, K. Burke and M. Ernzerhof, *Phys. Rev. Lett.*, 1996, **77**, 3865–3868.
41 K. Eichkorn, F. Weigend, O. Treutler and R. Ahlrichs, *Theor. Chem. Acc.*, 1997, **97**, 119–124.
42 F. Weigend, M. Häser, H. Patzelt and R. Ahlrichs, *Chem. Phys. Lett.*, 1998, **294**, 143–152.
43 F. Weigend and R. Ahlrichs, *Phys. Chem. Chem. Phys.*, 2005, **7**, 3297–3305.
44 B. Metz, H. Stoll and M. Dolg, *J. Chem. Phys.*, 2000, **113**, 2563–2569.
45 Y. Wang, J. Kröger, R. Berndt and W. Hofer, *Angew. Chem., Int. Ed.*, 2009, **48**, 1261–1265.
46 M. Toader and M. Hietschold, *J. Phys. Chem. C*, 2011, **115**, 3099–3105.
47 M. Lackinger and M. Hietschold, *Surf. Sci.*, 2002, **520**, L619–L624.
48 Y. Wang, J. Kröger, R. Berndt and H. Tang, *J. Am. Chem. Soc.*, 2010, **132**, 12546–12547.
49 A. Sperl, J. Kröger and R. Berndt, *J. Phys. Chem. A*, 2011, **115**, 6973–6978.
50 C. Stadler, S. Hansen, I. Kröger, C. Kumpf and E. Umbach, *Nat. Phys.*, 2009, **5**, 153–158.
51 J. D. Baran and J. A. Larsson, *J. Phys. Chem. C*, 2012, **116**, 9487–9497.
52 H. Marbach, *Acc. Chem. Res.*, 2015, **48**, 2649–2658.
53 A. Kretschmann, M. M. Walz, K. Flechtner, H.-P. Steinrück and J. M. Gottfried, *Chem. Commun.*, 2007, 568–570.
54 K. Diller, F. Klappenberger, F. Allegretti, A. C. Papageorgiou, S. Fischer, A. Wiengarten, S. Joshi, K. Seufert, D. Écija, W. Auwärter and J. V. Barth, *J. Chem. Phys.*, 2013, **138**, 154710.
55 K. Diller, F. Klappenberger, M. Marschall, K. Hermann, A. Nefedov, C. Wöll and J. V. Barth, *J. Chem. Phys.*, 2012, **136**, 014705.
56 M. Stark, S. Ditze, M. Lepper, L. Zhang, H. Schlott, F. Buchner, M. Röckert, M. Chen, O. Lytken, H.-P. Steinrück and H. Marbach, *Chem. Commun.*, 2014, **50**, 10225–10228.

 This journal is © the Owner Societies 2025

Open Access Article. Published on 05 May 2025. Downloaded on 22/11/2025 12:13:35 AM.
This article is licensed under a Creative Commons Attribution 3.0 Unported Licence.

57 C. Bürker, A. Franco-Cañellas, K. Broch, T. L. Lee, A. Gerlach and F. Schreiber, *J. Phys. Chem. C*, 2014, **118**, 13659–13666.
58 S. Ditze, M. Röckert, F. Buchner, E. Zillner, M. Stark, H.-P. Steinrück and H. Marbach, *Nanotechnology*, 2013, **24**, 115305.
59 S. Ditze, M. Stark, M. Drost, F. Buchner, H.-P. Steinrück and H. Marbach, *Angew. Chem., Int. Ed.*, 2012, **51**, 10898–10901.
60 C. M. Doyle, S. A. Krasnikov, N. N. Sergeeva, A. B. Preobrajenski, N. A. Vinogradov, Y. N. Sergeeva, M. O. Senge and A. A. Cafolla, *Chem. Commun.*, 2011, **47**, 12134–12136.
61 J. Xiao, S. Ditze, M. Chen, F. Buchner, M. Stark, M. Drost, H.-P. Steinrück, J. M. Gottfried and H. Marbach, *J. Phys. Chem. C*, 2012, **116**, 12275–12282.
62 M. Röckert, S. Ditze, M. Stark, J. Xiao, H.-P. Steinrück, H. Marbach and O. Lytken, *J. Phys. Chem. C*, 2014, **118**, 1661–1667.
63 M. Röckert, M. Franke, Q. Tariq, S. Ditze, M. Stark, P. Uffinger, D. Wechsler, U. Singh, J. Xiao, H. Marbach, H.-P. Steinrück and O. Lytken, *Chem. – Eur. J.*, 2014, **20**, 8948–8953.
64 R. González-Moreno, C. Sánchez-Sánchez, M. Trelka, R. Otero, A. Cossaro, A. Verdini, L. Floreano, M. Ruiz-Bermejo, A. García-Lekue, J. Á. Martín-Gago and C. Rogero, *J. Phys. Chem. C*, 2011, **115**, 6849–6854.
65 L. Smykalla, P. Shukrynau, D. R. T. Zahn and M. Hietschold, *J. Phys. Chem. C*, 2015, **119**, 17228–17234.
66 D. Sen, P. Błoński, B. de la Torre, P. Jelínek and M. Otyepka, *Nanoscale Adv.*, 2020, **2**, 2986–2991.
67 E. S. Frampton, M. Edmondson, C. J. Judd, D. A. Duncan, R. G. Jones and A. Saywell, *Inorg. Chim. Acta*, 2023, **558**, 121718.
68 B. Cirera, B. de la Torre, D. Moreno, M. Ondráček, R. Zbořil, R. Miranda, P. Jelínek and D. Écija, *Chem. Mater.*, 2019, **31**, 3248–3256.
69 M. Chen, M. Röckert, J. Xiao, H.-J. Drescher, H.-P. Steinrück, O. Lytken and J. M. Gottfried, *J. Phys. Chem. C*, 2014, **118**, 8501–8507.
70 J. Lu, B. Da, W. Xiong, R. Du, Z. Hao, Z. Ruan, Y. Zhang, S. Sun, L. Gao and J. Cai, *Phys. Chem. Chem. Phys.*, 2021, **23**, 11784–11788.
71 W. Xiong, X. Ren, B. Da, Y. Zhang, H. Zhang, J. Lu and J. Cai, *Phys. Chem. Chem. Phys.*, 2021, **23**, 18930–18935.
72 M. Pan, A. J. Brush, Z. D. Pozun, H. C. Ham, W. Y. Yu, G. Henkelman, G. S. Hwang and C. B. Mullins, *Chem. Soc. Rev.*, 2013, **42**, 5002–5013.
73 Y. Santiago-Rodríguez, J. A. Herron, M. C. Curet-Arana and M. Mavrikakis, *Surf. Sci.*, 2014, **627**, 57–69.
74 M. Pan, Z. D. Pozun, W. Y. Yu, G. Henkelman and C. B. Mullins, *J. Phys. Chem. Lett.*, 2012, **3**, 1894–1899.
75 A. Mairena, M. Baljozovic, M. Kawecki, K. Grenader, M. Wienke, K. Martin, L. Bernard, N. Avarvari, A. Terfort, K. H. Ernst and C. Wäckerlin, *Chem. Sci.*, 2019, **10**, 2998–3004.
76 R. Zuzak, A. Jančarík, A. Gourdon, M. Szymonski and S. Godlewski, *ACS Nano*, 2020, **14**, 13316–13323.
77 R. Zuzak, P. Dabczynski, J. Castro-Esteban, J. I. Martínez, M. Engelund, D. Pérez, D. Peña and S. Godlewski, *Nat. Commun.*, 2025, **16**, 691.
78 H. Okamoto and T. B. Massalski, *Bull. Alloy Phase Diagrams*, 1984, **5**, 276–284.
79 J. Homberg, A. Weismann and R. Berndt, *Phys. Rev. B*, 2024, **109**, 165426.
80 A. Banerjee, N. Ide, Y. Lu, R. Berndt and A. Weismann, *ACS Nano*, 2025, **19**, 7231–7238.